
**DEFORMATION
AND FRACTURE MECHANICS**

Simulation of the State of Stress in Locked-Coil Ropes during Tension and Torsion

V. F. Danenko^{a, *} and L. M. Gurevich^a

^a *Volgograd State Technical University, Volgograd, 400005 Russia*

^{*}*e-mail: omd@vstu.ru*

Received July 7, 2020; revised July 29, 2020; accepted August 11, 2020

Abstract—The state of stress in locked-coil rope elements is subjected to finite element simulation under joint tension and torsion. The axial forces and torques in the cross sections of the layers are found to be redistributed when a rope turns under an external torque, which leads to a decrease in the safety factor of the rope, a violation of the compatibility of the axial and radial displacements of the layers, and a violation of the structural integrity of the rope in the form of breaks in the outer layer wires.

Keywords: locked-coil rope, finite element simulation, state of stress, wire, profile, core, rope layer, tension, torsion, force, torque, equivalent stress, deformation, safety factor

DOI: 10.1134/S0036029521100128

INTRODUCTION

Multilayer locked-coil single spiral twist ropes are designed for the operation of a number of mechanisms of modern lifting and transport equipment. Locked-coil ropes are known to be used as the body of a pumping rod, which transmits the longitudinal force during reciprocating motion and the rotational motion from a surface drive to a deep-well pump during oil production from wells [1, 2]. The operability of ropes is largely determined by the stress and strain distribution in their elements (wires, layers), which depends on the technological parameters of manufacturing and the operating conditions of a rope.

The development of methods for an analysis of the state of stress (SOS) in multilayer wire structures is a challenging and practically significant problem. However, the number of works devoted to an experimental determination of the stresses in the elements of steel ropes on loading is scarce [3, 4], which is explained by the difficulty of access to the internal elements of the rope. An effective tool in solving the problem of ensuring the operability of multilayer ropes, which is not inferior in reliability to experimental and mathematical methods, is computer simulation of the SOS in ropes under loading [5–7].

The purpose of this work is to simulate the SOS in the locked-coil rope elements during axial tension and torsion, which imitate the transmission of the longitudinal force and rotational motion from a surface drive to a deep-well pump by a rope rod, in order to increase the reliability of predicting the static strength and reliability of the rope during operation.

FORMULATION OF THE PROBLEM

The SOS in the elements of a locked-coil rope during axial tension and torsion was studied by the finite element method using the licensed SIMULIA/Abaqus software package, which allowed us to obtain results at the necessary accuracy and performance [8]. The rope to be simulated consists of a 1 + 7 + 7/7 + 14 core made of round profile wires, next layer 4 of round wires, subsurface layer 5 of alternating round and H-profile wires, and outer layer 6 of Z-profile wires (Fig. 1a).

The single twist 1 + 7 + 7/7 + 14 core is made of round profile wires with axes in the form of helical lines, which are twisted in several layers around a central straight wire of diameter $d = 1.65$ mm (see Fig. 1). Layer 1 consists of 7 wires of the same diameter ($d = 1.23$ mm), layer 2 consists of alternating 7 wires of one diameter ($d = 1.18$ mm) and 7 wires of another diameter ($d = 0.9$ mm), and layer 3 consists of 14 wires of the same diameter ($d = 1.5$ mm). The cross sectional area of the core is 48.3 mm².

The core is twisted in one technological operation according to the linear touch principle: at the same layer twisting step ($t = 80$ mm), the wires of the layer lying above are placed in the recesses formed by the wires of the lower layer; the contact of the wire layers occurs along lines. The subsequent layers of the rope are twisted in separate technological operations according to the point touch principle with an alternating direction of twisting. Layer 4 consists of 16 round profile wires ($d = 1.9$ mm, $t = 145$ mm), layer 5 consists of alternating 14 round wires ($d = 1.87$ mm, $t = 130$ mm) and 14 H-profile wires ($h = 1.9$ mm), and layer 6 consists of 29 Z-profile wires ($h = 2.0$ mm, $t =$

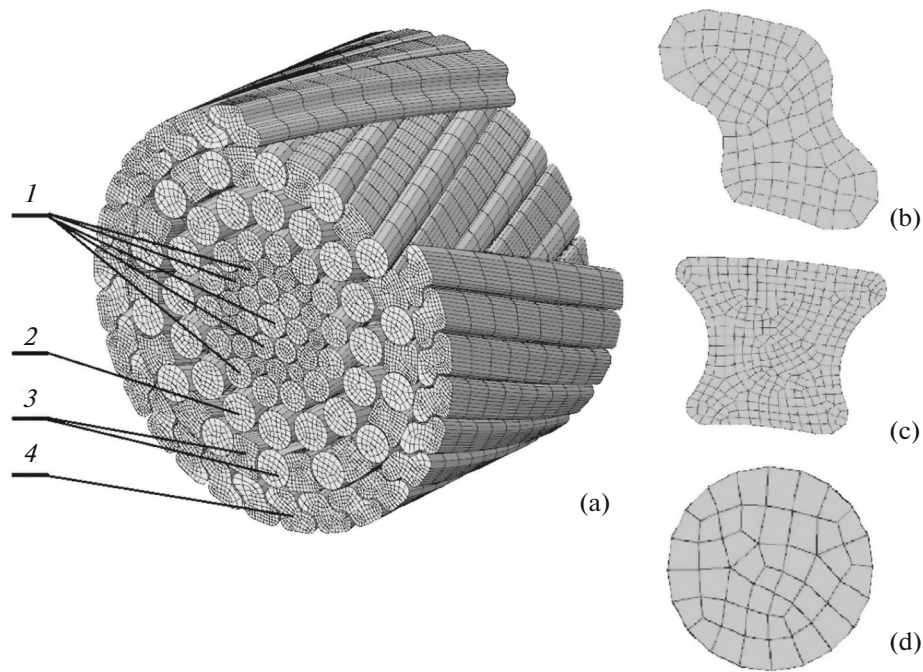


Fig. 1. Finite element simulation of a locked-coil rope and its elements: (a) cross section of the rope (part of the outer layer is conditionally removed), (b, c, d) Z-profile, H-profile and round-profile cross sections, respectively; (1) core (round wires); (2) layer 4 (round wires); (3) layer 5 (alternating round- and H-profile wires); and (4) layer 6 (Z-profile wires).

150 mm). In cross twisting, the wire layers contact at points. The cross sectional areas are 45.44 mm^2 for layer 4, 72.64 mm^2 for layer 5, and 104.05 mm^2 for layer 6.

The characteristics and dimensions of the rope elements used in the simulation are similar to those considered in [9]. When modeling all rope elements, we used cells of the C3D8R type, i.e., continuum three-dimensional eight-node reduced-integration elements. The cell length along the axis of the wires of all profiles was 1.5 mm, and the cell size in the cross section was 0.1 mm for the H-profile wires, 0.2 mm for the Z-profile ones, and 0.26–0.3 mm for the round-profile ones. The choice of the cell size was determined by the degree of curvature of individual profile elements. The spiral elements of the rope were formed by extrusion with a turn at a given step of the cross section of the wires, which led to a spiral twisting of a finite element mesh. The finite element mesh at the end of the wires is shown in Figs. 1b–1d.

The length of the simulated rope sample is $l_0 = 130 \text{ mm}$, the elastic modulus of the wire material is $E = 2 \times 10^5 \text{ MPa}$, and the friction coefficient is $\mu = 0.1$. The material of the rope wires was isotropic with strain resistance σ_s increasing with local plastic deformation, according to the curves shown in Fig. 2. As the wire material, we used steels of two groups of rated strength used for the manufacture of round and shaped-profile wires (1570 and 1370 MPa, respectively), with the following initial yield strengths: $\sigma_{s0} = 1120 \text{ MPa}$ for the

shaped profile (curve 1) and $\sigma_{s0} = 1280 \text{ MPa}$ for the round profile (curve 2).

The SOS characteristics of the elements of the spiral rope during tension and torsion were determined for two loading versions. According to the simulation version 1, the ends of the rope sample were fixed in devices to exclude their rotation at stage 1 and were tensioned at a rate of 4 mm/s to the axial force $P \approx 120 \text{ kN}$ (taking into account the load capacity of 80 kN and the mass of a 1500-m-long rope). At stage 2, the rope sample was subjected to torsion by external torque M in the direction leading to the unwinding of the outer layer of the Z-profile wires.

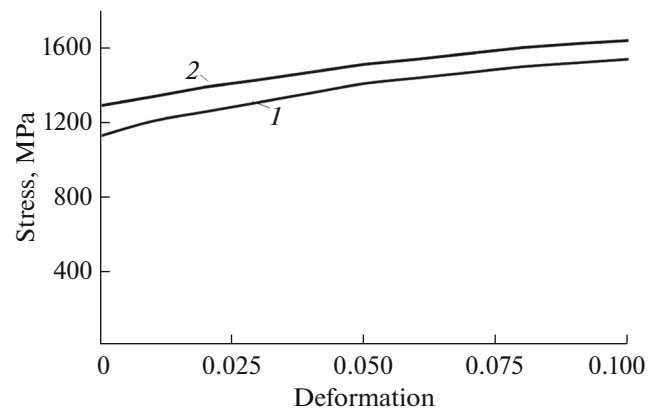


Fig. 2. Stress–strain curves of (1) H- and Z-profile and (2) round-profile wires.

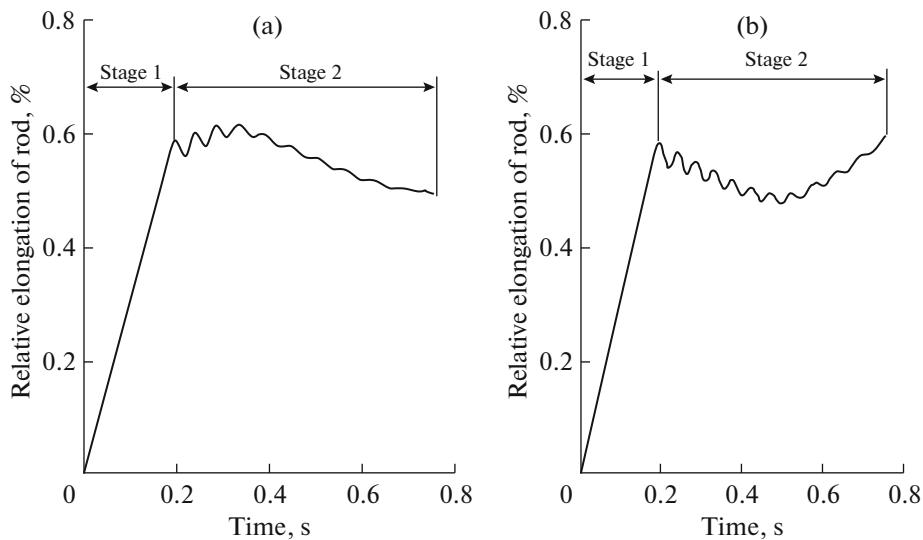


Fig. 3. Time dependence of the relative elongation of a rope sample for the simulation of loading for version (a) 1 and (b) 2.

According to simulation version 2, at stage 1, the sample was again tensioned without changing the loading conditions used in simulation version 1; at stage 2, the rope sample was twisted by external torque M in the direction opposite version 1, which led to the twisting of the outer layer of the Z-profile wires.

The unwinding (twisting) of the rope sample at stage 2 was carried out at a rate of 36 deg/s for 0.55 s (rotation angle is $\varphi \approx 20^\circ$) while maintaining external load P reached at stage 1. The direction of external torque M in the direction of twisting the outer layer of the rope sample was taken to be positive. At the same time, the loading scheme at stage 1 (pure tension: $\theta = 0$, $\varepsilon \neq 0$) was a model of longitudinal force transmission; at stage 2 (torsion under load: $\theta \neq 0$, $\varepsilon \neq 0$), the rotational motion from a surface drive to a deep-well pump was simulated [10].

To determine the loads and moments received by the rope layers during tension and subsequent torsion, the ends of the wire layers at the rear end of the simulated rope were firmly connected to the end surface of the movable hard disk of the equipment before tension; at the front end, they were connected to the coaxially arranged fixed rigid inner disk (1 + 7 + 7/7 + 14 core) and the rings (layers 4–6) [9]. The rope sample was deformed during tension by the axial motion of the movable hard disk, and the subsequent torsion was performed by the rotation of the movable hard disk at the achieved axial load (with the possibility of axial motion during rotation). The internal forces and moments in each layer were determined by the time-varying reactions at the supports on the fixed inner disk and the rings on the front end fixed at each simulation step.

The change in the equivalent Mises stresses σ_{equiv} in the cells of the finite element mesh was determined in the cross sections of the rope elements in the direction from the outer layer to the core. The sample size for

determining the average value of σ_{equiv} in the layer element was $n = 7–13$ depending on the element size (Figs. 1b–1d). The scatter of the values of σ_{equiv} in the cross section of the layer wires was estimated as confidence interval width $\Delta\sigma_{\text{equiv}}$ for the average value according to the formula

$$\Delta\sigma_{\text{equiv}} = \pm \frac{t(P, k)S}{\sqrt{n}},$$

where $t(P, k)$ is Student's test, $P = 0.95$ is the given confidence probability, $k = n - 1$ is the number of degrees of freedom, and S is the standard deviation of the sample values.

RESULTS AND DISCUSSION

Figure 3 shows the deformation curve of the rope sample during the gradual motion of the movable disk. For both versions at stage 1 (pure tension), the sample is elongated axially to a strain $\varepsilon \approx 0.6\%$. For simulation version 1 at the initial segment of stage 2 (rope unwinding), the relative elongation of the sample retains its value until the angle of rotation of the movable disk $\varphi = 5^\circ–6^\circ$, and it decreases to $\varepsilon \approx 0.5\%$ by the end of the stage (see Fig. 3a). For version 2 at stage 2 (rope twisting), the relative strain decreases initially, reaches a minimum ($\varepsilon \approx 0.5\%$) by the middle of the stage, and then increases (see Fig. 3b).

When analyzing the SOS of the sample for the accepted versions of external loading, we studied the distribution and magnitude of internal axial forces P and torques M_{tor} in the rope elements (Fig. 4, Table 1).

On simulating the pure tension at stage 1, the character of rope sample deformation at the beginning of loading and in the elastic elongation segment (see Figs. 4a, 4c; curves 5) is consistent with the data in [11]. The residual structural elongation of the sample

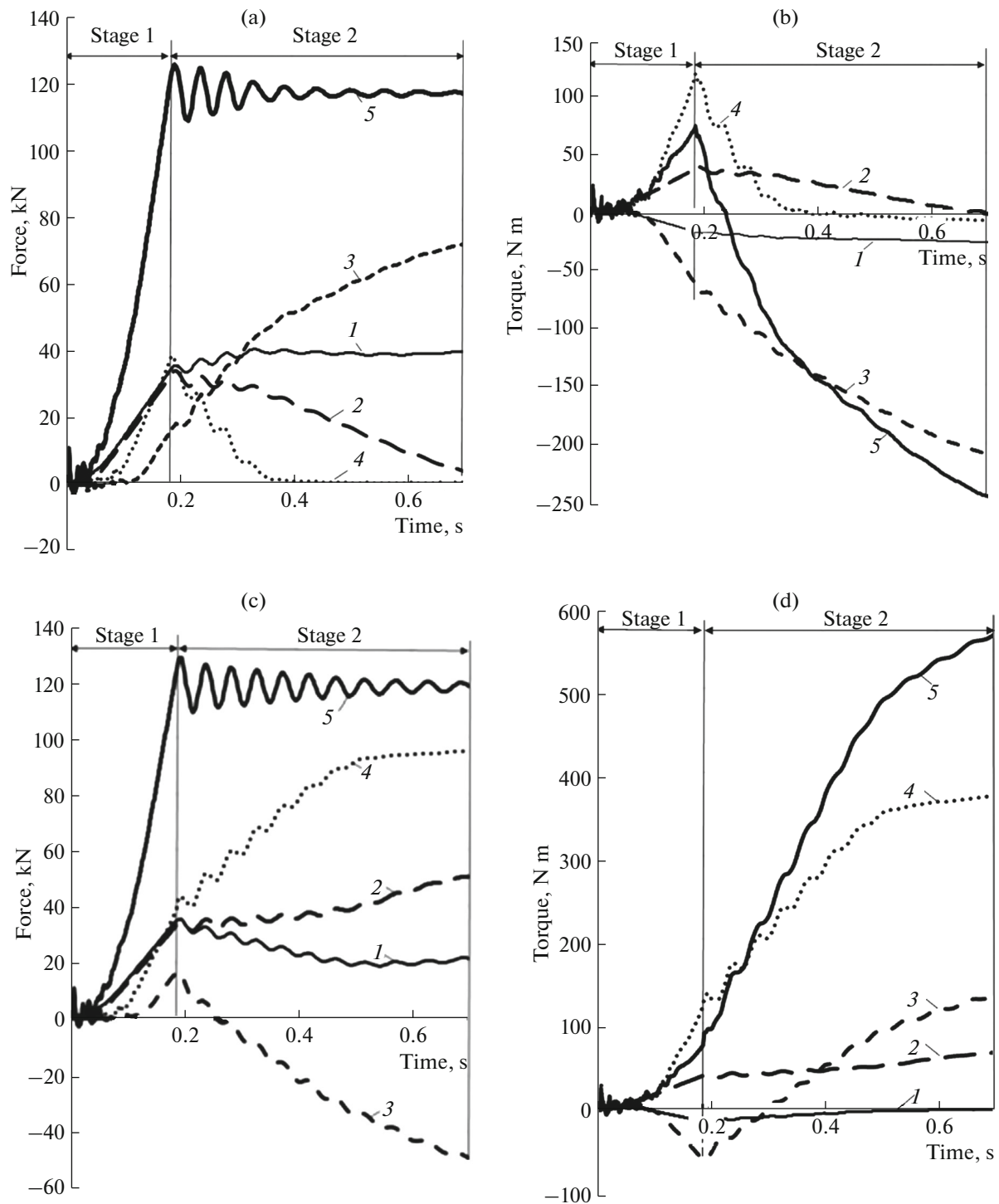


Fig. 4. Axial force and torque distributions in the rope and its layers during tension and torsion according to version (a, b) 1 and (c, d) 2: (1) core, (2) layer 4, (3) layer 5, (4) layer 6, and (5) rope.

associated with the running-in of the twisted wires at the corresponding decrease in the layer diameter is 0.24% of the length, which corresponds to the values recommended in [11]. The set tensile force $P \approx 120$ kN is within the elastic zone. The modulus of elasticity of the simulated rope, which is determined between two

fixed loads, is 1.4×10^5 MPa, which agrees with the data for locked-coil ropes [12].

At stage 1, the axial force distribution in the rope layers is nonuniform (see Figs. 4a, 4c), which is explained by the difference in the geometric param-

Table 1. Distribution of internal axial forces P , torques M_{tor} , and equivalent stresses σ_{equiv} in the cross sections of the rope elements at the accepted external loading parameters

Parameters	Core (round)	Layer 4 (round)	Layer 5 (round/H profile)	Layer 6 (Z profile)
Versions 1 and 2, stage 1 ($\varepsilon \neq 0, \theta = 0$)				
P , N	33740	32206	15324	36510
M_{tor} , N m	-17.1	35.3	-59.5	109.7
σ_{equiv} , MPa	687 ± 71.3	785 ± 25.7	$342 \pm 69.4/364 \pm 24.0$	392 ± 48.0
K	2.28	2.0	4.6/3.76	3.5
Version 1, stage 2 ($\varepsilon \neq 0, \theta \neq 0$)				
P , H	40869	2840	73307	905
M_{tor} , N m	-27.7	-4.6	-212.6	-7.5
σ_{equiv} , MPa	1030 ± 96.2	280 ± 73.2	$1240 \pm 54.7/1108 \pm 54.0$	201 ± 66.7
K	1.52	5.6	1.27/1.24	6.8
Version 2, stage 2 ($\varepsilon \neq 0, \theta \neq 0$)				
P , H	22127	51296	-51486	95918
M_{tor} , N m	-4.0	65.4	138.1	373.8
σ_{equiv} , MPa	353 ± 119.4	1270 ± 66.9	$731 \pm 246.0/731 \pm 131.6$	1155 ± 19.0
K	4.45	1.24	2.15/1.87	1.18

In parentheses, wire profile. Equivalent stresses σ_{equiv} and safety factor K in the core are given for layer 3.

ters (dimensions, shape, density of wire twisting) and in the mechanical properties of the screw elements. The lower tensile forces in layer 5 (curve 3), which has the highest residual structural elongation, are related to a delay in the formation of support surfaces to resist the circular compressive loads between the layer wires due to a significant initial total circumferential gap between them [9].

Axial tensile force P causes the elongation of the rope, which is accompanied by the unwinding of the spirally twisted layers, while internal torques M_{tor} appear in the cross sections of the layers. According to Figs. 4b and 4d and Table 1, torques M_{tor} increase in absolute value with the tensile force at stage 1. At the same time, the values of M_{tor} are negative for layer 5 (curve 3) and the core (curve 1) and are positive for layers 4 and 6 (curves 2 and 4), which is due to the opposite direction of layer winding. If the resulting torque is zero, the rope is balanced.

By the beginning of stage 2, the rope sample is in equilibrium under an external load $P \approx 120$ kN. When the rope turns under the action of an external torque M , internal forces P and torques M_{tor} are redistributed in the rope layers according to the law of additional stresses. Under the accepted conditions of fixing the ends of the layer wires with different directions of twisting to unmovable disks, the rope layers that tend to strongly change their dimensions axially during torsion transfer tensile forces to the layers that tend to weakly change their axial dimensions less, and vice versa.

In version 1 at stage 2, under the action of external torque M , the outer layer of the rope made of Z-profile wires is unwound. In this case, the wires of layer 5 and the core are compacted as a result of twisting and tend to decrease the axial layer length. Decreasing the length of the rope sample and maintaining the uniformity of the layer strain are prevented by unwinding layers 4 and 6. As a result, additional tensile stresses appear in layer 5 and the core, which leads to an increase in internal forces P and torques M_{tor} in absolute value (see Figs. 4a, 4b; curves 1, 3). In layers 4 and 6, compressive stresses appear and cause a decrease in internal forces P and torques M_{tor} in these layers (see Figs. 4a, 4b; curves 2, 4). The negative value of torque M_{tor} in layer 6 indicates the unwinding of this layer, which is confirmed by the results in [10] and indicates a possible separation of the rope and a multiple increase in the outer layer diameter.

In version 2 at stage 2, the rope is twisted under the action of external torque M . In this case, layers 4 and 6 are compacted and shorten as a result of twisting, which is prevented by unwinding layer 5 and the core. As a result, additional tensile stresses appear in layers 4 and 6, which leads to an increase in internal forces P (see Fig. 4c; curves 2, 4), and compressive stresses appear in layer 5 and the core and decrease internal forces P in these layers (see Fig. 4c; curves 1, 3). When the force in the core layers increases slightly, the internal force in layer 5 becomes compressive with an increase in the external moment and increases in absolute value. In general, when the rope sample is twisted, internal forces P and torques M_{tor} in layers 4–6

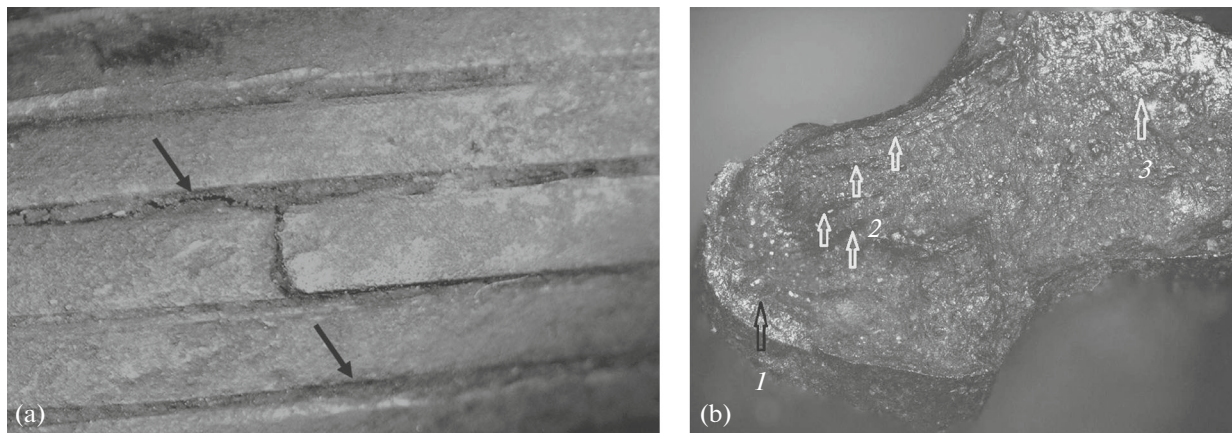


Fig. 5. (a) Appearance of the rope sample after operation and (b) fracture surface of the Z-profile wire. The arrows in (a) indicate the gaps between the wires formed during the operation of the rope; arrows 1, 2, and 3 in (b) indicate the zones of nucleation, stable crack growth, and rupture, respectively.

increase with the twisting angle (see Figs. 4c, 4d; curves 2–4).

To predict the static strength and reliability of the rope during operation, it is necessary to take into account the stress distribution in the cross section of the rope elements. By the end of stage 1, the equivalent stress σ_{equiv} distribution along the cross section of the rope is found to be nonuniform: the average of stresses in the central-layer wires of the rope increase (see Table 1). Layer 5 is less loaded. A comparison of the confidence interval width $\Delta\sigma_{\text{equiv}}$ demonstrates that the scatter of the equivalent stresses relative to the average stress in the sample is minimal in layer 4.

The application of external torque M at an achieved load $P \approx 120$ kN leads to stress σ_{equiv} redistribution in the rope elements at stage 2. For both versions, a non-uniform distribution of σ_{equiv} stresses over the cross section of the wire is characteristic of the untwisted layers, as indicated by the large confidence interval width σ_{equiv} for the average stresses (see Table 1). The stresses σ_{equiv} in the cross sections of the wires of the twisted layers are distributed more uniformly. For the outer layer of the Z-profile wires, the confidence interval width $\Delta\sigma_{\text{equiv}}$ is minimal; i.e., the scatter of the equivalent stresses is insignificant.

As follows from a comparison of the stresses σ_{equiv} for stages 1 and 2, the torsion of the rope causes an increase in the equivalent stresses in the twisted layers as compared to tension, which should affect the reliability of the rope during operation.

According to standards, the minimum safety factor of a rope is the ratio of the breaking force of the rope to the permissible load. The fact that the true SOS in the rope elements is unknown is compensated by high values of the safety factor, which are $K = 4.0$ – 6.0 depending on the operating conditions for lifting mechanisms [13]. In this paper, the safety factor of the rope layers was determined as the ratio of the permissible stresses in accordance with the rated group of a

wire to the average equivalent stresses σ_{equiv} over the cross section of the wire. For stage 2 of version 2, the values of coefficient K for twisted layers 6 and 4 are 1.18 and 1.24, respectively (see Table 1), which is on average 2.5–3.0 times lower than those for the rope when the safety margin is calculated using the highest tensile load. For the outer layer, we have $K = 1.2$ – 1.3 at rope rotation angles $\varphi = 10^\circ$ – 12° , which is explained by the distribution of axial force P and torque M_{tor} in the layer (see Figs. 4c, 4d; curve 4).

Low values of the safety factor increase the probability of breaking the wires of the outer layer of a locked-coil rope during operation. The causes of a breakage can be associated with the following factors: the surface defects formed during the manufacture of Z-profile wires by rolling [4, 14], the influence of an external aggressive environment accelerating fatigue failure [15–19], and the experimentally detected non-uniformity of the stress distribution in the Z-profile wires [20]. The possibility of breaks is confirmed by the results of studying the violation of the structural integrity of a locked-coil rope [9, 10] after operation as a pump rod body in the wells of OOO LUKOIL-PERM [2]. The nature of the breakage of the Z-profile wires in the outer layer of the rope is shown in Fig. 5. Note that the outer surface of the rope was subjected to external corrosion during operation and to the displacement of individual Z-profile wires during alternating loading of the rope with the formation of inter-wire gaps (shown by the arrows in Fig. 5a). The failure of the Z-profile wire began from the lower shelf (zone 1) and ended on the upper shelf (zone 3). The focus of crack formation in zone 1 indicates that the local stresses exceeding the yield strength of the metal appeared at this point in the cross section of the wire. High equivalent stresses, along with possible surface defects and a nonuniform external stress distribution in the rope elements, led to the destruction of the Z-profile wires of the outer layer of the rope.

CONCLUSIONS

(1) According to the results of finite element simulation of the SOS in the elements of a locked-coil rope under axial tension and torsion, the distribution of internal axial forces P and torques M_{tor} in the rope elements under pure tension is nonuniform. The subsequent turns of the rope under the action of an additional applied external torque M lead to an increase in the nonuniformity of the force P and torque M_{tor} distribution in magnitude and sign in the rope elements. The maximum axial forces and torques appear in the twisted layers, which increases the SOS in them. Here, conditions are created for the implementation of axial and radial displacements different in layers, which can cause a violation of the structural integrity of the rope.

(2) An external torque causes equivalent stresses σ_{equiv} in the rope, which are higher as compared to the stage of axial tensile effects. This fact is reflected on the result of the rope safety margin estimation: the safety factor of the outer layer in twisting is 2.5–3.0 times lower than that recommended by standards and is $K = 1.2$ –1.3 at rope rotation angles $\varphi = 10^\circ$ – 12° .

(3) Finite element simulation of the SOS in the elements of multilayer spiral ropes during joint tension and torsion allowed us to determine the true SOS of the rope elements at the stage of designing, to optimize the design and technological parameters of twisting to increase the safety factor of the wires, and to ensure the durability and reliability of ropes during operation.

REFERENCES

1. V. N. Ivanovskii, A. A. Sabirov, A. V. Degovtsov, and S. S. Pekin, "Rope pumping rod," RF Patent 2527275, Byull. Izobret., No. 24 (2014).
2. V. N. Ivanovskii, A. A. Sabirov, A. V. Degovtsov, S. S. Pekin, S. G. Patrushev, E. V. Kachin, and S. V. Popov, "Experience of operation of wells with small-diameter side shafts, SpSNU with a cable rod in OOO LUKOIL-PERM," Territoriya NEFTEGAZ, No. 3, 78–87 (2015).
3. N. G. Kulik, "Experimental study of the stresses in steel rope elements," in *Steel Ropes* (Tekhnika, Kiev, 1968), pp. 199–201.
4. S. V. Polyakov, "Investigation of a lifting rope with changes in the geometric parameters and mechanical properties of screw elements," Nauch.-Tekhn. Vestn. Bryansk Gos. Univ., No. 2, 257–264 (2019).
5. Y. Yu, Z. Chen, H. Liu, and X. Wang, "Final element study of behavior and interface force conditions of seven-wire strand under axial and lateral loading," Constr. Build. Mater. **66**, 10–18 (2014).
6. V. Fontanari, M. Benedetti, and B. D. Monelli, "Elasto-plastic behavior of a Warrington–Seale rope: experimental analysis and finite element modeling," Eng. Str. **82**, 113–120 (2015).
7. V. V. Tarasov, E. A. Kalent'ev, and V. N. Novikov, "Steel ropes. Calculation of structures and evaluation of operational properties," in *Mechanics and Physical Chemistry of Heterogeneous Media, Nanosystems, and New Materials* (IM UrO RAN, Izhevsk, 2015), pp. 237–259.
8. O. V. Antonova, A. S. Nemov, I. B. Voinov, P. S. Goncharov, and A. I. Borovkov, "Finite element analysis of ropes. Comparison of software systems Abaqus, LS-DYNA, MSC, and MARC," in *Proceedings of All-Russian Conference of Students and Postgraduates XXXVI Science Week of SPbGPU* (Izd. SPbGPU, St. Petersburg, 2009). <http://elibr.spbstu.ru/dl/007906.pdf>.
9. V. F. Danenko and L. M. Gurevich, "Modeling of the influence of tension on the structural integrity of lifting locked-coil ropes," Materialoved., No. 2, 43–48 (2020).
10. V. F. Danenko, L. M. Gurevich, and I. R. Myazina, "Radial displacements of lifting locked-coil rope elements during their joint tension and torsion," Izv. VolgGTU, No. 10 (233), 68–74 (2019).
11. A. P. Koshkin and G. D. Trifanov, *Ropes for Lifting Installations* (Izd. PNIPU, Perm, 2014).
12. M. A. Bukshtein, *Production and Use of Steel Ropes* (Metallurgiya, Moscow, 1973).
13. *RTM 24.0909–77. Lifting Cranes. Cargo Lifting Mechanisms. Calculation Methods* (Izd. NIIinformtyazhmash, Moscow, 1978).
14. V. F. Danenko, E. Yu. Kushkina, T. S. Kubrakova, G. V. Ponkratova, and E. O. Gul'tsev, "Development of technology for manufacturing shaped wire on an FPW 200-6 rolling mill," Chern. Met., No. 10, 38–43 (2013).
15. V. N. Ivanovskii, A. V. Degovtsev, A. A. Sabirov, Sh. A. Aliev, O. V. Tret'yakov, I. I. Mazein, A. V. Usenkov, S. V. Merkushev, and D. N. Krasnoborov, "Analysis of the probability of failure-free operation of deep-well pump systems with a cable rod in the fields of OOO LUKOIL-PERM," Territoriya NEFTEGAZ, No. 7–8, 74–80 (2017).
16. P. M. Galimov, F. I. Dautov, and S. A. Dolgikh, "An integrated approach to the protection of equipment from internal corrosion," Nefteprom. Delo, No. 5, 29–63 (2007).
17. K. Gjerding-Smith, R. Johnsen, H. I. Lange, B. H. Leinum, G. Gundersen, B. Isaksen, and G. Nærum, "Wire fractures in locked coil cables," Bridge Str. **2** (2), 63–77 (2006).
18. R. Betti, C. A. West, G. Vermaas, and Y. Cao, "Corrosion and embrittlement in high-strength wires of suspension bridge cables," J. Bridge Eng. **10** (2), 151–162 (2005).
19. N. N. Sergeev, A. N. Sergeev, S. N. Kutepov, A. G. Kolmakov, and A. E. Gvozdev, "Mechanisms of hydrogen cracking of metals and alloys. Part I (review)," Materialoved., No. 3, 27–33 (2018).
20. N. N. Plodovitev, "Stress distribution in the outer layer of the wires of a carrier rope during its tension," in *Steel Ropes* (Tekhnika, Kiev, 1966), pp. 195–196.

Translated by K. Shakhlevich